Mathematical modeling suggests high potential for the deployment of floating photovoltaic on fish ponds

Pierre-Alexandre Château [a], Rainer F. Wunderlich [a], Teng-Wei Wang [b], Hong-Thih Lai [b], Che-Chun Chen [b,*], Fi-John Chang [a,*]

[a] Department of Bioenvironmental Systems Engineering, National Taiwan University, Taiwan
[b] Department of Aquatic Bioscience, National Chiayi University, Taiwan

HIGHLIGHTS

- Floating photovoltaic (FPV) allows harnessing solar energy in land-scarce areas.
- We present a calibrated model of a fish pond ecosystem subject to FPV covering.
- Monte Carlo runs show a beneficial trade-off between fish and energy productions.
- FPV has the potential to significantly contribute to Taiwan's national energy mix.

GRAPHICAL ABSTRACT
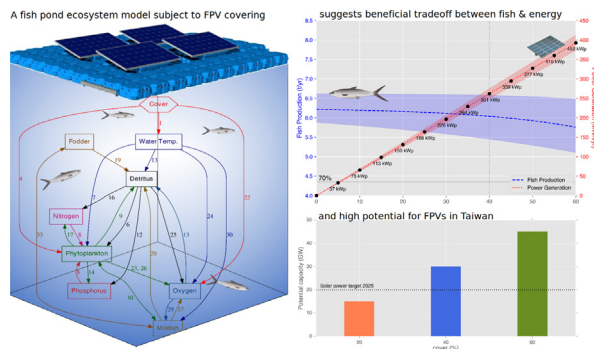
ABSTRACT

Rising energy needs and pressure to reduce greenhouse gas emissions have led to a significant increase in solar power projects worldwide. Recently, the development of floating photovoltaic (FPV) systems offers promising opportunities for land scarce areas. We present a dynamic model that simulates the main biochemical processes in a milkfish (*Chanos chanos*) pond subject to FPV cover. We validated the model against experimental data collected from ponds with and without cover during two production seasons (winter and summer) and used it to perform a Monte-Carlo analysis of the ecological effects of different extents of cover. Our results show that the installation of FPV on fish ponds may have a moderate negative impact on fish production, due to a reduction in dissolved oxygen levels. However, losses in fish production are more than compensated by gains in terms of energy (capacity of around 1.13 MW/ha). We estimated that, with approximately 40,000 ha of aquaculture ponds in Taiwan, the deployment of FPV on fish ponds in Taiwan could accommodate an installed capacity more twice as high as the government's objective of 20 GW solar power by 2025. We argue that the rules and regulations pertaining to the integration of FPV on fish ponds should be updated to allow realizing the full potential of this new green technology.

© 2019 Published by Elsevier B.V.

1. Introduction

Growing demand for water, food and energy requires an integrated framework to sustainably manage these vital resources (Endo et al.,

2015; Endo et al., 2017; Zisopoulou et al., 2018; Zhou et al., 2019). The Water-Food-Energy (WFE) nexus raises a holistic vision that intends to strike a balance among the diverse targets, interests and demands of people as well as the environment (Hamiche et al., 2016; Giupponi and Gain, 2017; Kurian, 2017). Technical solutions that make use of synergies along the water-food, water-energy, and food-energy boundaries are currently being explored worldwide to reduce waste and improve global sustainability (Bieber et al., 2018; Hanes et al., 2018; Lin et al., 2018; Tian et al., 2018; Uen et al., 2018; Yao et al., 2018).

In this context, photovoltaic (PV) energy is considered to be one of the most promising sources of energy due to its ubiquity and sustainability (Sahu et al., 2016; Loik et al., 2017). However, PV has a large footprint area which reduces the amount of land available for agricultural purposes (Trapani and Millar, 2013). In the recent years, floating photovoltaic (FPV) or floatovoltaics, has emerged as a potential solution to the problem of land scarcity (Trapani and Redón Santafé, 2015; Kougias et al., 2016). The implementation of FPV systems can trigger powerful synergies between energy production, water conservation and food production (Pringle et al., 2017) thereby contributing to the optimization of the WFE nexus. A review of existing projects shows increasing trends for both the scale (in MW) and the number of FPV installations (Trapani and Redón Santafé, 2015). Several articles have presented the technological and economic viability of FPV systems (Ferrer-Gisbert et al., 2013; Santafé et al., 2014; Sahu et al., 2016; Cazzaniga et al., 2018), and reported better FPV performances than conventional ground-based PV installations thanks to the cooling effect of water (Choi, 2014; Ho et al., 2015; Da Silva and Branco, 2018; Liu et al., 2018). FPV has also been shown to reduce water evaporation (Santafé et al., 2014; Taboada et al., 2017) and improve water quality by limiting algal proliferation (Chang et al., 2014; Lu et al., 2015).

The application of FPV systems on aquaculture ponds (aquavoltaics) would greatly extend the area where the production of renewable energy becomes feasible. Numerous studies have developed mathematical models of fish pond ecosystems (Piedrahita et al., 1984; Svirezhev et al., 1984; Wolfe et al., 1986; Li and Yakupitiyage, 2003; Zhang et al., 2017; Granada et al., 2018), but to our knowledge, the ecological effects of covering fish ponds with floating solar panels have not yet been studied. It is generally acknowledged that the shading provided by the panels is likely to reduce the growth of photosynthetic organisms, and may therefore have a negative impact on herbivorous fish via trophic cascade effects. On the other hand, the solar cover may protect farmed fish from predatory birds (Pringle et al., 2017). While the floatovoltaics industry is booming, the lack of study on the ecological effects of covering fish ponds with solar panels is hindering the development of aquavoltaics.

Here, we propose to discuss these effects with a case study from Taiwan. More specifically, through a modeling approach, we simulate the effects of different FPV covers on water quality and fish production in a milkfish pond. The milkfish (*Chanos chanos*) is the only living species in the family Channidae. It is distributed across the Indo-Pacific but limited to coastal waters in the vicinity of continental shelves and oceanic islands, and to warm water temperatures (Bagarinao, 1994). It is the most important aquaculture species in Southeast Asia with global annual production exceeding one million tonnes since 2013 of which 50,000 t are farmed in Taiwan (http://www.fao.org/fishery/culturedspecies/Chanos_chanos/en).

Following the Fukushima disaster, the Taiwanese government has launched a nuclear power phase-out program to the horizon 2025. Although the complete phase out by 2025 was rejected in the 2018 Taiwanese referendum, a long term transition to renewable energies was still broadly supported. The government has stated an objective of 20 GW installed PV systems by 2025, including FPV systems. Current regulations regarding the installation of FPV on fish ponds are derived from regulations for ground-based PV systems on agricultural land. These stipulate that the percentage of land covered with solar panels cannot exceed 40% of the land parcel and that agricultural production

has to be maintained above 70% of its former value. These rules assume that agricultural production and solar energy are mutually exclusive. While this might be true for ground-based PV systems vs. agricultural production, it is possible that FPV systems be deployed on aquaculture ponds without causing such reductions in fish production. To quantify the trade-off between fish harvest and energy generated, we ran different FPV cover scenarios, thereby describing a production frontier between fish and energy. We then discuss the current regulations pertaining to the installation of FPV on fish ponds in Taiwan, and suggest that these should be updated to allow for higher covers. Finally, we assess the total capacity in Taiwan if all fish ponds were equipped with FPV.

2. Materials and methods

2.1. Study framework

The mathematical model built for this study describes the biochemical processes that occurs in a typical Taiwanese milkfish pond. Field measurements were performed in two different ponds, during two production cycles (winter and summer). The collected data was used for model validation. After validation, the model was used to explore the effects of different FPV covers on the fish pond ecosystem. Finally, energy simulations were combined with the fish simulations to provide an assessment of the integrated production of fish and energy. Fig. 1 summarizes the framework of this study.

2.2. Model description

The model we present is mainly derived from Svirezhev et al. (1984) and subsequent work by Voinov and Svirezhev (1984) and Voinov and Akhremenkov (1990). Fig. 2 displays the causal links that compose the model structure. Our model features eight ordinary differential
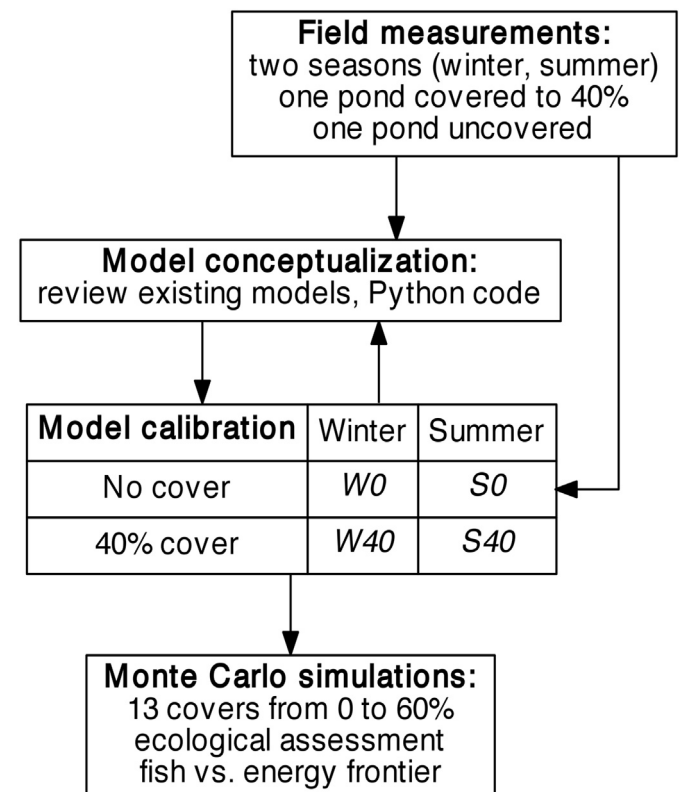
Fig. 1. Study flowchart.
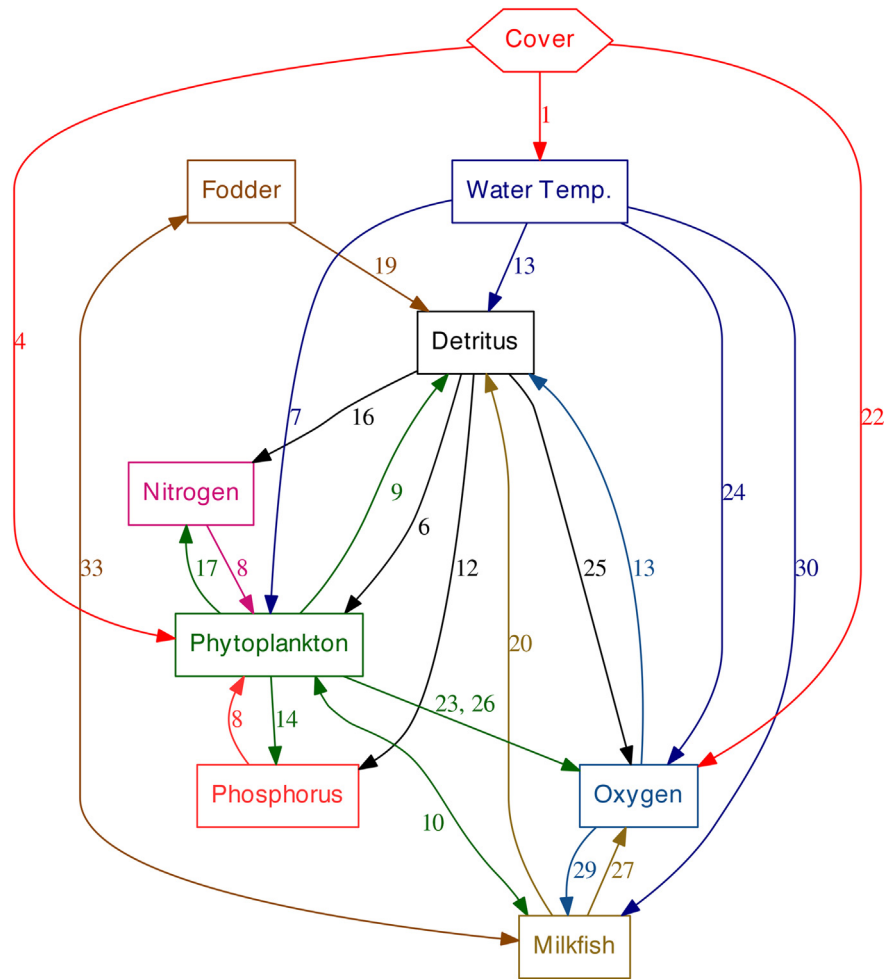
Fig. 2. Structure of the fish pond ecosystem model. State variables are shown in rectangle boxes. Each arrow is colored as the variable it comes from and is associated with the corresponding equation number.

equations (ODEs): water temperature (WT), phytoplankton (F), nitrogen (N), phosphorus (P), detritus (D), dissolved oxygen (DO), artificial fodder (A) and milkfish (M). These ODEs are connected to form a dynamic system that describes major ecological processes such as photosynthesis and respiration, nutrient cycling, and milkfish growth, while including environmental variables such as global radiation, ambient air temperature and wind speed. The modeled ponds being shallow (depth < 2 m), small (approximately 4000 m^2) and well-mixed, we neglect the effects of the spatial distribution of organisms, nutrients and detritus. All simulated variables are regarded as concentrations measured in mg/L. For milkfish, this means we used the ratio of their total biomass to the volume of the pond. State variables are shown within brackets in the following equations.

2.2.1. Water temperature

WT tends towards air temperature (AT, in °C) by convection, and during the day, it increases with global radiation (GR, in MJ/m^2). We assumed that under covering, both gases exchanges between surface water and the atmosphere and solar radiation decline following the exponential decay function $exp(-cover)$ (Eqs. (1) & (2), Fig. 3a). The idea behind this formulation is that gases exchanges and received light will never decline to the point where they are equal to zero, even under 100% cover. The speed at which convection occurs at the surface of the pond varies with wind speed (WS, in m/s) and the use of water mixers. Usually, more water mixers are turned on during nighttime than during

daytime (Eq. (2)). In the experiment ponds, two water mixers were used during the day and four during the night.

ODE for WT

$$\frac{d[WT]}{dt} = mixin * wt_a * (AT-[WT]) + wt_b * GR * \exp(-cover) \qquad (1)$$

Water turbulence

$$mixin = \begin{cases} mix_{base} + mix_{mixer} * 2 + mix_{wind} * WS * \exp(-cover), & if\ GR = 0 \\ mix_{base} + mix_{mixer} + mix_{wind} * WS * \exp(-cover), & else \end{cases} \qquad (2)$$

2.2.2. Phytoplankton

F increases with growth and decreases with grazing by fish and natural mortality (Eq. (3)). F growth rate (Eq. (4)) is calculated as the product of FL, the light limitation function (Eq. (5), Fig. 3d), FT_F, the temperature limitation function (Eq. (7), Fig. 3b) and the Holling Type II uptake of nutrients (Eq. (8)). Under cover, only a fraction of F biomass is exposed to light, growth is finally scaled down accordingly (Fig. 3a). The consumption of F by M follows an Holling Type II trophic function (Eq. (10)). Natural mortality is proportional to F and constitutes the flow from F to D (Eq. (9)).
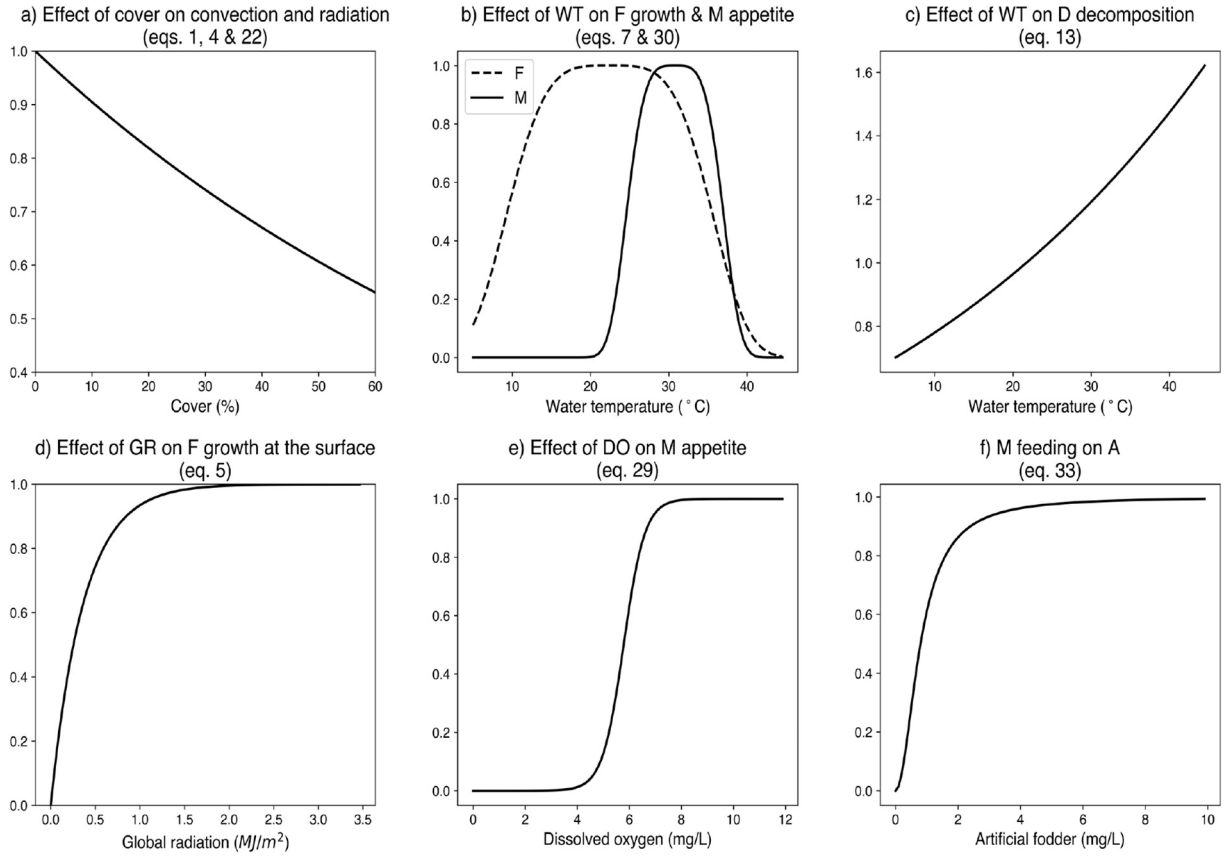
Fig. 3. Effects of cover on convection and radiation (a), water temperature on phytoplankton growth (F) and fish appetite (M) (b), water temperature on detritus decomposition (c), global radiation on phytoplankton growth (d), dissolved oxygen on fish appetite (e), and fish feeding on artificial fodder (f).

ODE for F

$$\frac{d[F]}{dt} = GF - FD - FM \tag{3}$$

F growth

$$GF = \mu_F^{max} * FL * FT_F * \ min(V_F([P]), V_F([N])) * [F] * \exp(-cover) \tag{4}$$

Light effect on GF [0; 1]

$$FL = 1 - \exp(-c_L * GR * \ \exp(-k * h)) \tag{5}$$

Light extinction coefficient

$$k = kw + kf * [F] + kd * (1 - \exp(-C_{SS} * mixin)) * [D] \tag{6}$$

WT effect on GF [0; 1]

$$FT_F = \ \exp\left(-slp_F^{FT} * \left(\frac{t_F^{opt} - [WT]}{t_F^{opt} - t_F^{min}}\right)^4\right) \tag{7}$$

N & P effects on GF [0; 1]

$$V_F(N) = \frac{[N]^2}{K_{NF}^2 + [N]^2}, V_F(P) = \frac{[P]^2}{K_{PF}^2 + [P]^2} \tag{8}$$

F mortality

$$FD = m_F * [F] \tag{9}$$

M consumption of F

$$FM = \mu_{FM}^{max} * FO_M * FT_M * V_M([F]) * [M] \tag{10}$$

2.2.3. Nitrogen & phosphorus

N and P are formed by the decomposition of D. The strength of this process increases with WT following a Van't-Hoff function (Fig. 3c) and with DO following an asymptotic exponential function. We assumed that only the suspended fraction $1-exp(-C_{SS}*mixin)$ of D (i.e. Suspended Solids, SS) is decomposed, while the remaining part is trapped temporarily in the sediments (Eq. (13)). Releases of N and P are calculated by multiplying the N:P stoichiometric ratio of D (dn:dp) with the fraction of D being decomposed (Eqs. (12) & (16)). Similarly, the uptake of N and P by F is proportional to F growth and the N:P stoichiometric ratio of F (fn:fp, Eqs. (14) & (17)).

ODE for N

$$\frac{d[N]}{dt} = DN - NF \tag{11}$$

Fraction of decomposed D that turns into N

$$DN = dn * DX \tag{12}$$

D decomposition

$$DX = ds * 2^{\frac{[WT]-p1}{p2}} * (1 - \exp(-c_D * [DO])) * (1 - \exp(-C_{SS} * mixin)) * [D] \tag{13}$$

N uptake by F

$$NF = fn * GF \tag{14}$$

ODE for P

$$\frac{d[P]}{dt} = DP - PF \qquad (15)$$

Fraction of decomposed D that turns into P

$$DP = dp * DX \qquad (16)$$

P uptake by F

$$PF = fp * GF \qquad (17)$$

2.2.4. Detritus

D increases with the destruction of A (Eq. (19)), mortality of F (Eq. (10)) and excretion of M (Eq. (20)). It decreases with decomposition (Eq. (13)).

ODE for D

$$\frac{d[D]}{dt} = AD + FD + MD - DX \qquad (18)$$

Flow from A to D

$$AD = alpha * [WT] * [A] \qquad (19)$$

M excretion

$$MD = mb_M * (AM + FM) \qquad (20)$$

M consumption of A

$$AM = \mu_{AM}^{max} * FO_M * FT_M * V_M([A]) * [M] \qquad (21)$$

2.2.5. Dissolved oxygen

DO is driven by both physical and biological processes (Eq. (22)). As WT always tends towards AT, DO always tends towards its saturated value (O_{sat}), defined following Wang et al. (1978) (Eq. (24)), owing to surface layer exchanges with the atmosphere. The rate at which it does so is proportional to the turbulence rate (mixin, Eq. (2)) and the percentage of cover (Fig. 3a). During daytime, DO increases with photosynthesis Eq. (23)). For oxygen consumption, we sum the consumption of oxygen by the oxidation of detritus (Eq. (25)), F respiration (Eq. (26)) and M respiration (Eq. (27)).

ODE for DO

$$\frac{d[DO]}{dt} = FO + mixin * rea * (O_{sat} - [DO]) - OD - OF - OM \qquad (22)$$

F production of DO

$$FO = phot * GF \qquad (23)$$

Saturated DO

$$O_{sat} = 14.61996 - 0.4042 * [WT] + 0.00842 * [WT]^2 - 0.00009 \\ * [WT]^3 \qquad (24)$$

Bacterial consumption of DO

$$OD = resp_D * DX \qquad (25)$$

F consumption of DO

$$OF = resp_F * (1 - \exp(-[DO])) * [F] \qquad (26)$$

M consumption of DO

$$OM = resp_M * ME \qquad (27)$$

M respiration

$$ME = mbo_M * FO_M * FT_M * [M] \qquad (28)$$

DO effect on fish appetite [0; 1]

$$FO_M = \frac{1}{1 + \exp\left(slp_M^{FO} * \left(mid_M^{FO} - [DO]\right)\right)} \qquad (29)$$

WT effect on ME [0; 1]

$$FT_M = \exp\left(-slp_M^{FT} * \left(\frac{t_M^{opt} - [WT]}{t_M^{opt} - t_M^{min}}\right)^4\right) \qquad (30)$$

2.2.6. Artificial fodder

A increases with FA, the feeding as practiced by the farmer. As a rule, the farmer checks the pond everyday at 11 am, appraises the amount of fodder that remains in the pond and inputs the complement of it to the amount of fodder deemed necessary (Eq. (32)). FO_M (Eq. (29), Fig. 3e) and FT_M (Eq. (30), Fig. 3b) determine fish appetite as functions of DO and WT respectively. Together and along with the abundance of A (Eq. (33), Fig. 3f), these functions determine the fish consumption of fodder (Eq. (21)).

ODE for A

$$\frac{d[A]}{dt} = FA - AD - AM \qquad (31)$$

A input

$$FA = \begin{cases} feed_M * [M] - [A], & if\ hour = 11am \\ 0, & else \end{cases} \qquad (32)$$

M feeding on A [0; 1]

$$V_M([A]) = \frac{[A]^2}{K_{AM}^2 + [A]^2} \qquad (33)$$

2.2.7. Fish

Milkfish growth is simulated as the difference between the fish consumption of fodder (Eq. (21)), the fish consumption of phytoplankton (Eq. (9)), fish excretion (Eq. (20)) and fish respiration (Eq. (28)). The growth process is scaled by a logistic component that represents the effect of fish density on fish growth and imposes a carrying capacity (K_M) on the pond (Eq. (34)).

ODE for M

$$\frac{d[M]}{dt} = (AM + FM - MD - ME) * \left(1 - \frac{[M]}{K_M}\right) \qquad (34)$$

2.2.8. Other variables

Biological Oxygen Demand (BOD, Eq. (35)) and chlorophyll-a (Chl-a, Eq. (36)) were calculated from SS and F respectively for calibration to experimental data. A conversion factor of 0.015 mg Chl-a per mg phytoplankton was used (Smith and Piedrahita, 1988).

BOD

$$BOD = resp_D * (1 - \exp(-C_{SS} * mixin)) * [D] \qquad (35)$$

Chl-a

$$Chl\!-\!a = 0.015 * [F] \tag{36}$$

2.3. Study site

The model was validated using data obtained from experiments conducted in Chiayi county, southern Taiwan, where water quality was sampled from two milkfish ponds: one not covered and the other covered up to 40% with an Hydrelio polyethylene floating solar system by Ciel & Terre (described in Sahu et al. (2016) and Silvério et al. (2018), shown on Fig. 4). Water quality parameters were sampled in both ponds every two weeks and included *Chl-a*, *N*, *P*, *BOD*, and *SS*. *Chl-a* was estimated with the Shimadzu spectrophotometer UV-1800. Analysis methods of *N* (including ammonia, nitrite and nitrate), *P*, *BOD* and *SS* were performed following the regulation methods of the Environmental Protection Administration, Taiwan, R.O.C. (https://wq.epa.gov.tw). A real-time monitoring system (model QAM300-DE by Quadlink Technology Inc.) was installed in both ponds to collect *WT* and *DO* every hour. Weather data from Chiayi city (hourly *AT*, *GR* and *WS*) were collected from the Central Weather Bureau (http://e-service.cwb.gov.tw/HistoryDataQuery).

2.4. Model implementation and calibration

The model was implemented in Python 2.7 (https://www.python.org) and calibrated against four scenarios using the PEST (Parameter EStimation) software (Doherty, 2010). Simulations were conducted on a Ubuntu 16.04 system with an Intel Core i5-4440 Processor and 8 GB RAM. The runtime for a five-months scenario with a one-hour time-step is approximately 0.8 s. Scenarios run and their corresponding data are shown in Table 1.

The four scenarios (W0, S0, W40 and S40) correspond to the experiments conducted in Chiayi. Two ponds (no cover and 40% cover) were sampled over a period of time that spanned over two sessions of fish culture (winter, from October 2017 to April 2018 and summer, from April 2018 to September 2018). A set of 43 model parameters (Appendix 1) was estimated so that the total agreement of the model with the four datasets was maximized. Also, a regularization constraint was added to the objective function to prevent the estimated parameters from moving too far from their reference values (Doherty and Skahill, 2006).

Energy output was simulated using the NREL's PVWatts DC power model (Dobos, 2014) as implemented in the PVLIB Python library (Stein et al., 2016). We ran the simulation for two five-months fish culture sessions (the winter and summer sessions exclude the coldest and warmest months of February and August), assuming the use of Neo Solar Power (D6P310B4A) 310 W solar panels.

3. Results and discussion

3.1. Experimental data

Summary statistics (means and standard deviations) of experimental datasets are displayed in Table 2. Student's independent samples test is performed for each variable, in both seasons to determine if their means are significantly different without cover (W0 and S0) than under 40% cover (W40 and S40).

Experimental data suggests that covering the pond significantly reduced average *DO* and *WT*. For other variables, the lower number of data points available hinders the significance of the tests, but suggests reduced average *BOD*, *Chl-a*, *SS*, and *N*, and increased average *P*. For *M*, the effect of covering seems dependent on the season since the average size of harvested fish in the covered pond was higher than in the not covered one during winter and lower during summer.

3.2. Calibration results

Estimated parameters are given with their 95% confidence intervals in Appendix 1. Reference values were collected from the literature, notably from Svirezhev et al. (1984) and Voinov and Akhremenkov (1990). Overall, the model satisfactorily simulates the trends observed in the ponds ecosystems in all four scenarios. Fig. 5 shows the agreement between calibrated results and experimental data. The correlation coefficient (r) between predicted and observed values across the 32 variables-scenarios ranges from −0.212 (*P*—W40) to 0.993 (*M*-S0). Its average is 0.55. The Mean Absolute Percentage Error (MAPE) ranges from 0.03 (*WT*-S0) to 1.95 (*N*—S40). Average MAPE is 0.41.

Fig. 4. Experimental pond with 40% cover.

Table 1
Data collected for the multi-scenarios calibration.

Winter		Summer	
No cover	40% cover	No cover	40% cover
W0	W40	S0	S40
DO (1433 obs.)	DO (1402 obs.)	DO (2102 obs.)	DO (1551 obs.)
WT (1427 obs.)	WT (1393 obs.)	WT (2100 obs.)	WT (1551 obs.)
BOD (6 obs.)	BOD (6 obs.)	BOD (6 obs.)	BOD (6 obs.)
Chl-a (8 obs.)	Chl-a (8 obs.)	Chl-a (6 obs.)	Chl-a (6 obs.)
M (3 obs.)	M (3 obs.)	M (3 obs.)	M (3 obs.)
SS (6 obs.)	SS (6 obs.)	SS (6 obs.)	SS (6 obs.)
N (8 obs.)	N (8 obs.)	N (6 obs.)	N (6 obs.)
P (6 obs.)	P (6 obs.)	P (6 obs.)	P (6 obs.)

3.3. Ecological effects of covering

We simulated the impact of increasing cover on fish pond ecosystem in winter (from September 1st to January 31st) and summer (from March 1st to July 31st), using average weather data from Chiayi city (hourly air temperature, wind speed and global radiation) over the period 2010–2018. We assumed that, in order to maintain access to the farmed fish, the cover would not exceed 60% of the pond area. We ran 1000 Monte-Carlo simulations per cover scenario starting at 0% (no cover) up to 60% cover with increments of 5% (13 cover scenarios), for both winter and summer seasons (total of 26,000 runs, performed in around 5.4 h) by randomly sampling within the parameters 95% confidence intervals. We used uniform distributions to draw the random parameters values. Fig. 6 shows the ecological effects of 20%, 40% and 60% covers as compared to no cover, for both winter and summer sessions.

In both winter and summer, increasing cover was associated with reductions in DO, WT, BOD, chl-a, M, and SS, but increases in nutrients N and P. These results are in line with experimental data except for N, which was lower in the covered pond (Table 2).

The magnitude of observed changes was dependent on the season. In winter, high cover (60%) led to stronger reductions in BOD, chl-a, M and SS than in summer. Conversely, increases in N and P were higher in summer than in winter. This pattern can be best explained by the fact that due to higher global radiation, F growth can be sustained to a higher level in summer than in winter and therefore BOD, SS and nutrients are maintained at higher levels. During our simulations, P was the limiting nutrient for F growth about 80% of the time. This is the reason why P is kept in better check than N.

3.4. Trade-off between fish and energy

Fig. 7 shows fish production vs. energy generation for different covers, for winter and summer seasons. Shown data points are averages

from the Monte-Carlo simulations. The envelope represents the standard deviation.

Due to higher GR, the most productive season for both fish and energy is summer. With increasing cover, power generation increases proportionally but fish harvest declines. Average DO being lower under high cover than without cover (Fig. 6), the resulting reduction in fish appetite hinders fish growth (Fig. 3e). This effect is especially strong during daytime (Fig. 8), when fish usually feed. The cooling effect of the cover further reduces appetite (Fig. 3b) when WT is lower than the optimal temperature for milkfish (estimated at 31.8 °C). Accumulated over a five months period, these effects lead to an estimated reduction in fish production of 10% in winter and 5% in summer, under 60% cover.

3.5. Potential for integrated production

The moderate impact of covering the pond on fish growth suggests that there is high potential for the integrated production of fish and energy. Fig. 9 displays the fish-energy trade-off over two consecutive production cycles. Two dotted lines are added to represent the current regulation constraint on integrated production: cover cannot exceed 40% and at least 70% of fish production has to be maintained.

Under 60% cover, fish production still largely remains above the 70% production target. A modification of the actual "40% cover / 70% fish" regulation to a "60% cover/70% fish" regulation would lead to a decrease of around 444 kg/yr in fish production and an increase of energy of around 130 MWh/yr. The feed-in tariffs (FIT) rate for floating solar in 2018 is 0.155 USD/kWh (https://www.moea.gov.tw/MNS/english/news/News.aspx?kind=6&menu_id=176&news_id=76457), and the price of milkfish in Taiwan is currently around 2.692 USD/kg (https://m.coa.gov.tw/outside/AquaticTrans/Search.aspx). Given this set of prices, it is easy to see that the additional production of energy (20,150 USD/yr) largely compensates for the reduction in fish production (−1197 USD/yr) and that substantial economic gains can be made by applying FPV to the highest possible extent. The annual revenue from a pond with 20% (150 kWp), 40% (301 kWp) and 60% (452 kWp) coverage could potentially increase 2-, 4- and 5-fold respectively.

In most situations in Taiwan, the farmer doesn't own the pond in which he farms fish. Interests may therefore diverge between land owner and farmer. While the owner might be tempted to invest in solar panels, the farmer would likely oppose the installation of a FPV system that complicates pond operations and reduces his harvest. A financial system aiming at compensating the farmer for losses should therefore be implemented in order to ensure that the gains are fairly shared by both parties.

With a total aquaculture area of approximately 40,000 ha in Taiwan (https://www.fa.gov.tw/en/FisheriesoROC/content.aspx?id=2&chk=05d9ffd2-651d-4686-a2d1-a44413152366&param=pn%3D1), a policy that would promote the massive adoption of FPV systems on aquaculture ponds could generate a very significant power output. Fig. 10 shows the potential installed capacity (GW) if all ponds in Taiwan

Table 2
Experimental results.

Variable	Mean W0	Mean W40	Winter t-test		Mean S0	Mean S40	Summer t-test	
DO (mg/L)	8.35 ± 1.83	7.49 ± 1.34	t(28) = 3.25**	–	6.99 ± 2.63	6.1 ± 1.38	t(32) = 2.45*	–
WT (°C)	20.99 ± 3.83	20.22 ± 3.32	t(28) = 5.34***	–	31.03 ± 1.95	29.63 ± 1.76	t(32) = 12.61***	–
BOD (mg/L)	17.28 ± 11.96	15.35 ± 5.05	t(5) = 0.39	–	21.07 ± 9.04	15.37 ± 5.32	t(5) = 2.59*	–
Chl-a (mg/L)	1.61 ± 0.38	1.06 ± 0.46	t(7) = 2.78*	–	1.06 ± 0.35	0.86 ± 0.26	t(5) = 1.2	–
SS (mg/L)	106.61 ± 58.37	77.55 ± 27.52	t(5) = 1.24	–	103 ± 36.16	56.05 ± 14.82	t(5) = 3.9*	–
M (g/ind.)	88.78 ± 28.37	104.26 ± 7.05	t(11) = −2.15	–	623.3 ± 255.3	611.35 ± 130.9	t(11) = 0.1	–
N (mg/L)	10.42 ± 4.45	7.61 ± 3.74	t(5) = 1.35	–	4.39 ± 2.09	1.8 ± 1.02	t(5) = 3.01*	–
P (mg/L)	2.51 ± 1.09	2.93 ± 1.69	t(5) = −1.61		3.88 ± 0.94	6.53 ± 0.63	t(5) = −5.28**	–

* Significant at $p < 0.05$.
** Significant at $p < 0.01$.
*** Significant at $p < 0.001$.
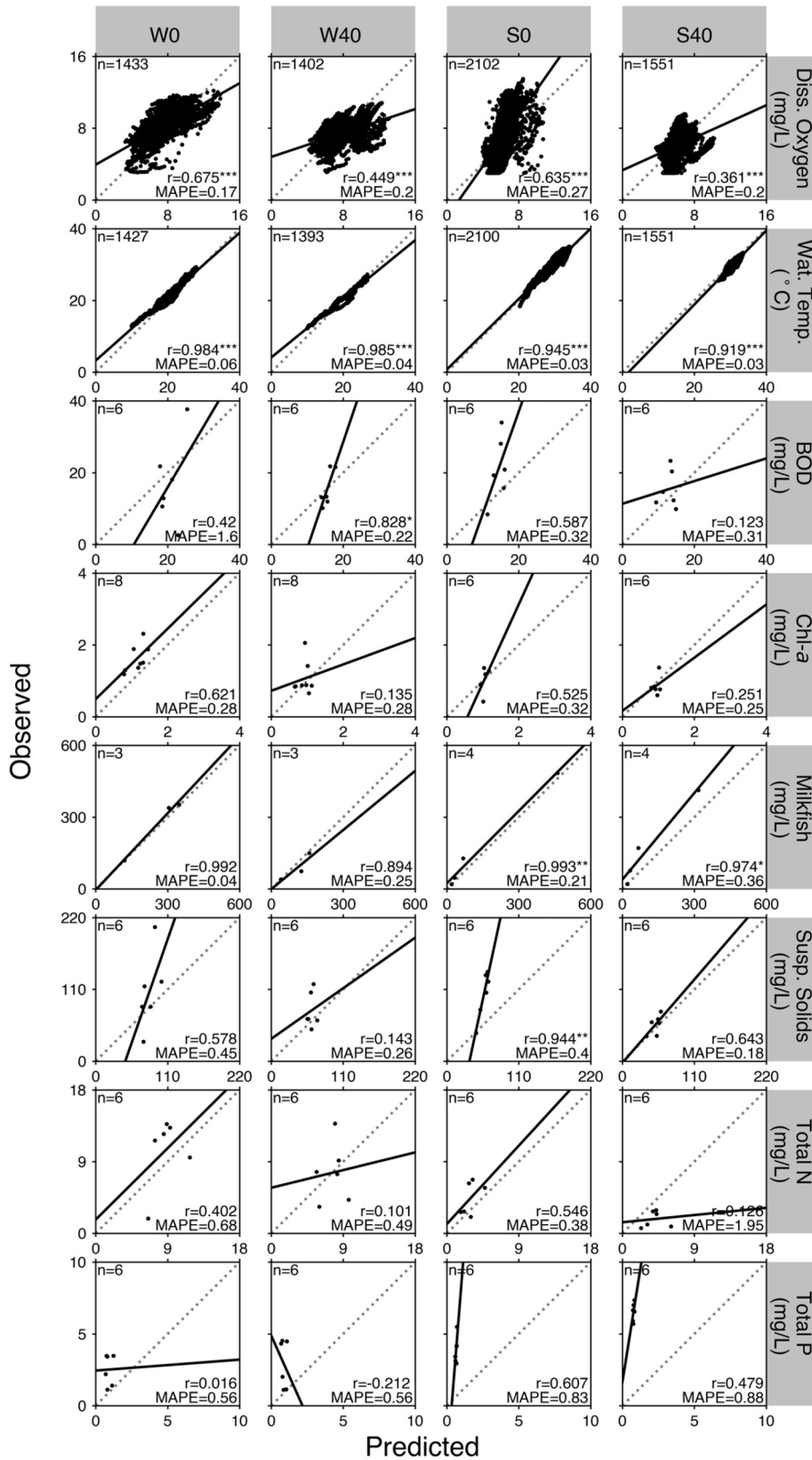
Fig. 5. Model results (x-axis) vs. experimental data (y-axis) for DO, WT, BOD, Chl-a, M, SS, TN and TP in calibration scenarios W0, S0, W40 and S40. *: r significant at $p < 0.05$, **: r significant at $p < 0.01$, ***: r significant at $p < 0.001$.

were covered up to 20%, 40% and 60% respectively, assuming homogeneous global radiation in Taiwan.

This assessment for Taiwan appears to be quite conservative when compared with a study that estimated the potential capacity of an
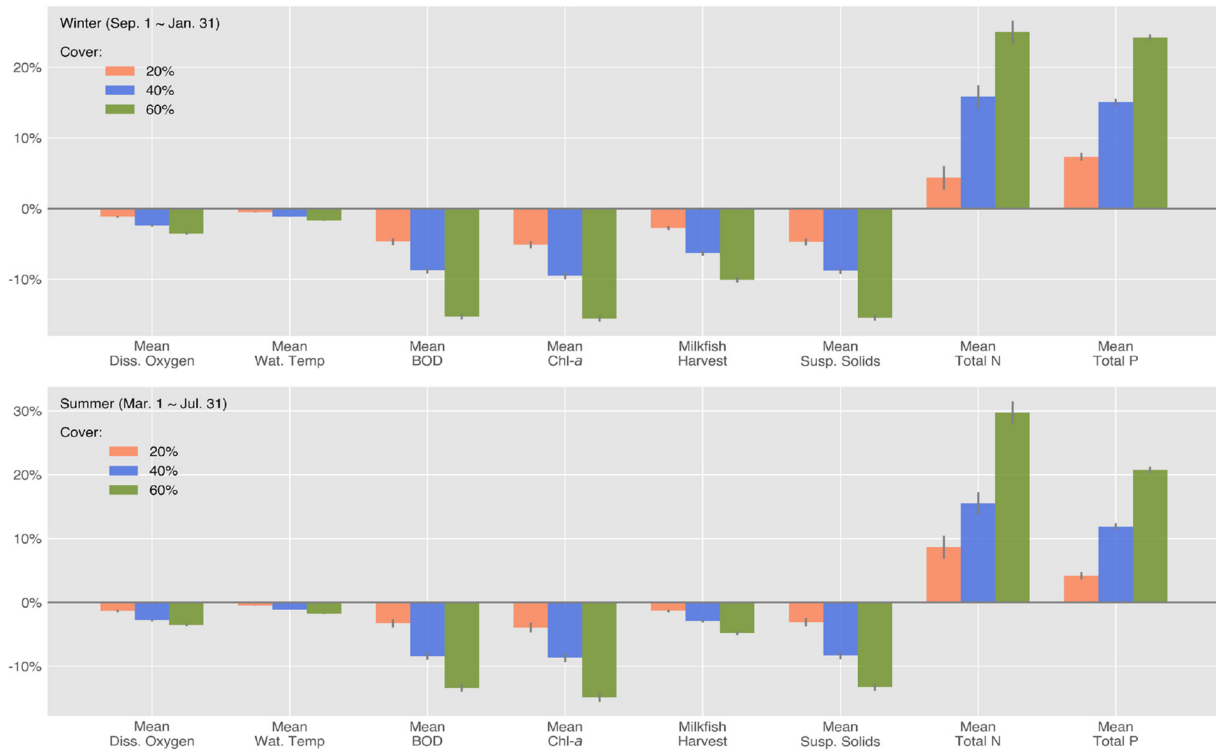
Fig. 6. Average ecosystem changes under 20% (orange), 40% (blue), 60% (green) covers, in winter (upper panel) and summer (lower panel). (For interpretation of the references to color in this figure legend, the reader is referred to the web version of this article.)

average 27% FPV cover on 2,196,138 ha water bodies in the United States to be 2116 GW (Spencer et al., 2019).

3.6. Model limitations and future work

Our model provides a platform for simulating the effects of different FPV covers on a typical Taiwanese milkfish pond. To our knowledge, this
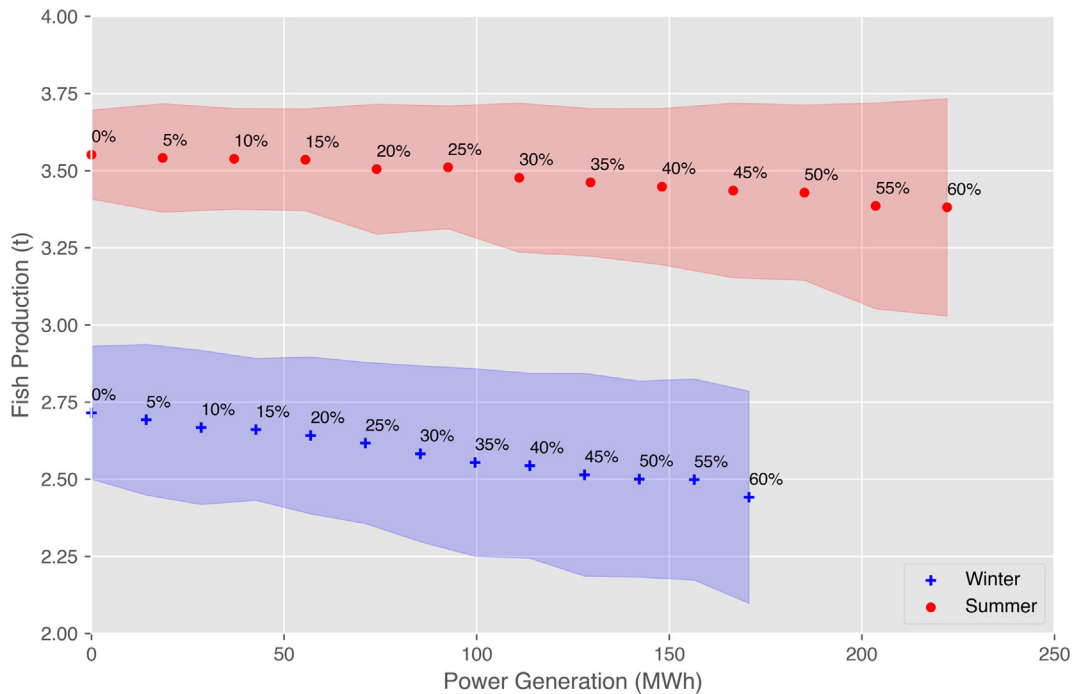
Fig. 7. Fish-Energy production frontier in winter (blue) and summer (red). Percentage cover is added above simulated points. (For interpretation of the references to color in this figure legend, the reader is referred to the web version of this article.)
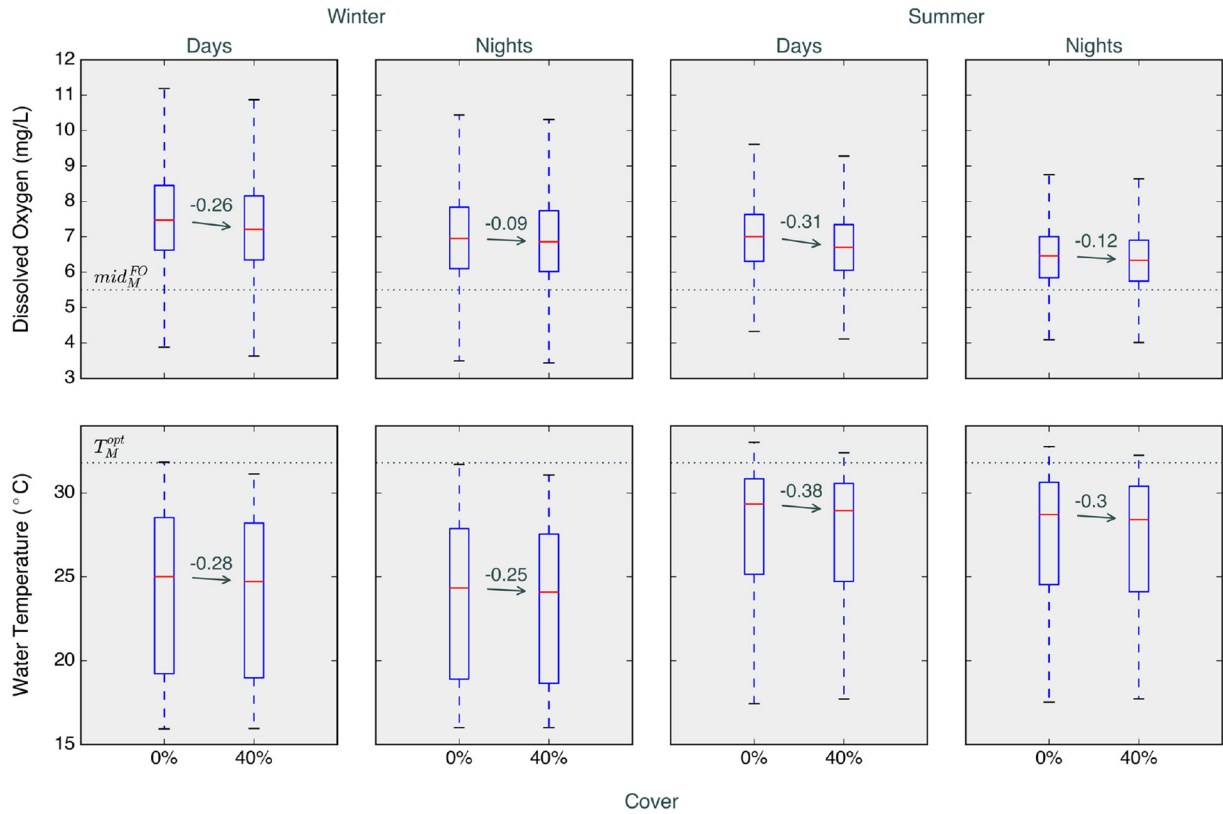
Fig. 8. Dissolved Oxygen (upper panel) and Water Temperature (lower panel) during winter days, winter nights, summer days and summer nights (from left to right) for all runs without and with 40% cover (outliers not shown).The difference between medians is reported on each subplot.

is the first of its kind to explore the potential synergies at work in aquavoltaics. We showed that the model performance was satisfying when compared with experimental data. However, the assessment of model performance was hindered by the low data availability for some of the model variables. In the future, we should collect experimental data more frequently. Also, an experimental setup with more varying covers, such as no cover, 20, 40 & 60%, would allow for a more robust description of the impacts of covering.

It is well known that ammoniacal nitrogen (NH3-N) is toxic to fish (Thurston et al., 1981; Handy and Poxton, 1993; Ip et al., 2001) and more specifically to milkfish (Cruz, 1981; Sumagaysay, 1998). The assimilation of ammonia by phytoplankton is an important process to control the amount of ammonia in fish ponds (Durborow et al., 1997). Therefore, the reductions in phytoplankton biomass and increases in total nitrogen that are predicted with increasing covers could lead to an increased toxicity for fish. In light of these considerations, a revision
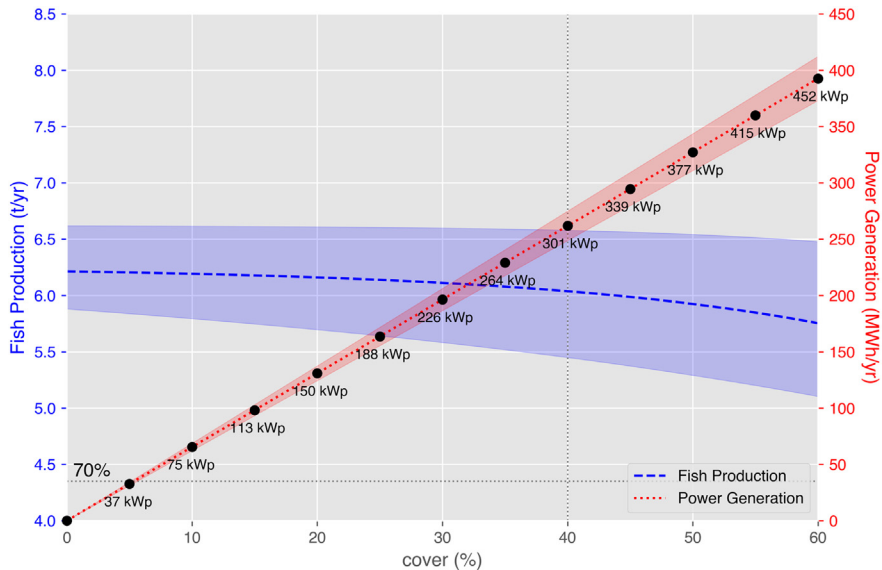
Fig. 9. Fish Production (blue) and Power Generation (red) over a year. Installed FPV nominal power is added below simulated Power Generation points. (For interpretation of the references to color in this figure legend, the reader is referred to the web version of this article.)
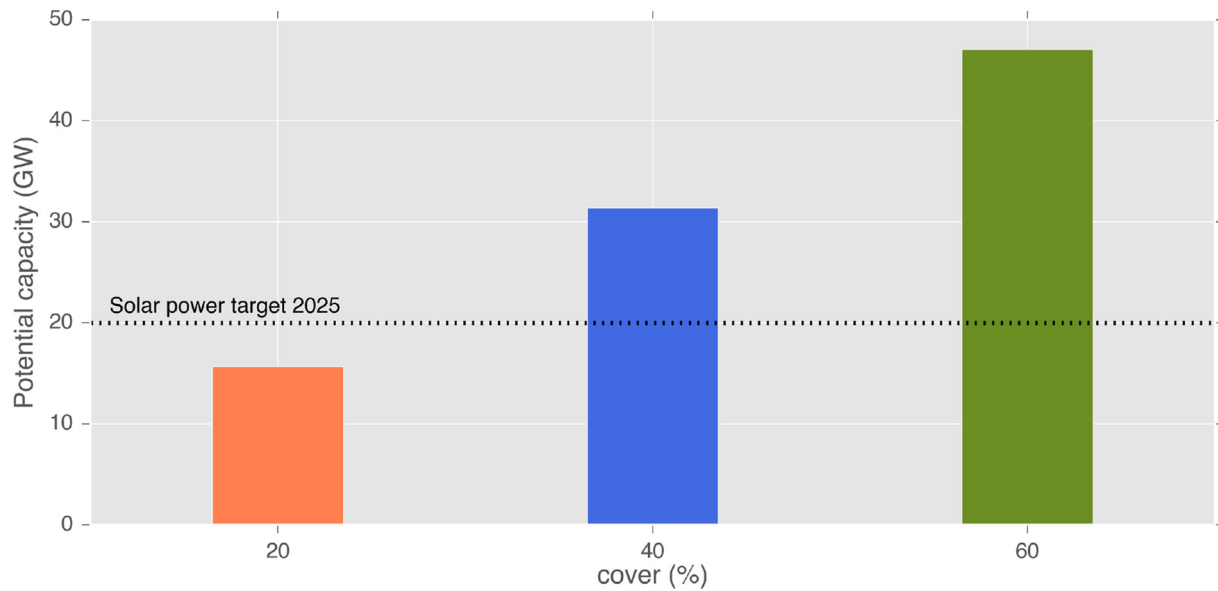
Fig. 10. Potential installed capacity if all aquaculture ponds in Taiwan were covered up to 20% (orange), 40% (blue) and 60% (green). (For interpretation of the references to color in this figure legend, the reader is referred to the web version of this article.)

of the model should be performed to better describe the nitrogen cycle and the different forms of nitrogen (ammonia, nitrate and nitrite) and their impacts on fish.

The calculations regarding the revenues that can be derived from aquavoltaics only account for the sales (of fish and electricity). The investment cost of the FPV is not accounted for. In Taiwan, it is usually said that the amortization of such an installation takes between 6 and 8 years. Further analysis should be done to assess the economics of aquavoltaics.

4. Conclusion

We present a mathematical model of an aquaculture fish pond subject to FPV cover. The model was calibrated using experimental data from two ponds (without and with 40% cover), in two production seasons (winter and summer). Simulation results suggest a highly beneficial trade-off between power generation and fish production. We showed that it is possible to cover up to 60% while still maintaining more than 70% fish production. Using the 2018 FIT rate for solar energy

and the current market price of milkfish, we calculated that annual revenues from a 4000 m^2 milkfish pond could increase up to 5-fold under 60% cover. We also estimated that the potential installed capacity for FPV on aquaculture ponds can reach up to 45 GW, more than twice as much as the government's goal for all solar power by 2025. We hope these results can help decision-makers promote the development of FPV systems for a more sustainable future.

Appendix 1. Model parameters

Name	Unit	Reference	Estimated	95%min	95%max
alpha	1/day	1.00E-02	3.71E-03	3.32E-03	4.16E-03
C_D	dmnl	5.00E-01	1.42E00	1.09E00	1.85E0 0
C_L	dmnl	2.00E00	2.80E00	2.40E00	3.27E0 0
C_{SS}	dmnl	5.00E-01	6.56E-01	5.65E-01	7.61E-01
ds	1/day	1.00E-01	3.78E-01	3.35E-01	4.27E-01
dn	%	1.30E-01	1.06E-01	1.04E-01	1.08E-01
dp	%	8.00E-03	9.79E-03	9.60E-03	9.99E-03
$feed_M$	mg/l	4.00E-02	4.43E-02	4.29E-02	4.58E-02
fn	%	1.30E-01	1.06E-01	1.04E-01	1.08E-01
fp	%	8.00E-03	9.95E-03	9.75E-03	1.02E-02
h	m	1.00E-01	8.77E-02	7.58E-02	1.01E-01
K_{AM}	mg/l	3.00E00	9.30E-01	8.60E-01	1.01E0 0
K_{FM}	mg/l	2.00E00	2.11E00	1.94E00	2.30E0 0
K_M	mg/l	5.00E02	5.00E02	/	/
kd	dmnl	2.00E-02	1.53E-01	1.44E-01	1.63E-01
kf	dmnl	8.00E-03	1.14E-02	8.67E-03	1.50E-02
kw	dmnl	8.00E-02	1.20E-01	9.39E-02	1.54E-01
K_{NF}	mg/l	1.00E00	5.21E00	4.93E00	5.51E0 0
K_{PF}	mg/l	1.00E00	1.66E00	1.55E00	1.78E0 0
mb_M	dmnl	3.00E-01	1.01E-01	8.51E-02	1.21E-01
mbo_M	1/day	1.00E-03	4.76E-03	3.76E-03	6.01E-03

(*continued*)

Name	Unit	Reference	Estimated	95%min	95%max
m_F	1/day	4.00E-01	3.01E-01	2.84E-01	3.19E-01
mid_M^{FO}	mg/l	3.00E00	5.50E00	5.39E00	5.62E-0
mix_{base}	dmnl	1.00E-01	7.92E-02	6.05E-02	1.04E-01
mix_{mixer}	dmnl	1.00E00	5.14E-01	4.46E-01	5.92E-01
mix_{wind}	dmnl	1.00E00	1.12E00	9.79E-01	1.28E0 0
$p1$	°C	2.00E01	2.45E01	1.92E01	3.13E0 1
$p2$	°C	1.00E01	3.48E01	2.87E01	4.21E0 1
$phot$	1/day	1.00E00	2.16E-01	2.05E-01	2.26E-01
rea	1/day	3.00E-01	2.70E-01	2.36E-01	3.10E-01
$resp_D$	1/day	8.50E-02	2.53E-01	2.42E-01	2.65E-01
$resp_F$	1/day	1.00E-03	1.22E-03	9.15E-04	1.62E-03
$resp_M$	1/day	1.00E-02	1.26E-02	9.53E-03	1.68E-02
slp_M^{FO}	dmnl	1.00E00	2.78E00	2.14E00	3.60E0 0
slp_F^{FT}	dmnl	1.00E00	5.71E-01	4.81E-01	6.78E-01
slp_M^{FT}	dmnl	3.00E00	1.47E01	1.36E01	1.59E0 1
T_F^{min}	°C	1.00E01	1.01E01	9.95E00	1.02E0 1
T_M^{min}	°C	1.60E01	1.75E01	1.73E01	1.77E0 1
T_F^{opt}	°C	2.30E01	2.25E01	2.22E01	2.28E0 1
T_M^{opt}	°C	2.70E01	3.18E01	3.14E01	3.22E0 1
wt_a	dmnl	1.60E-01	1.79E-01	1.53E-01	2.09E-01
wt_b	°C/MJ-m^2	2.80E00	1.26E00	1.12E00	1.42E0 0
μ_{AM}^{max}	1/day	3.00E-02	6.29E-02	5.66E-02	6.99E-02
μ_F^{max}	1/day	4.00E00	7.76E00	7.04E00	8.55E0 0
μ_{FM}^{max}	1/day	3.00E-03	1.00E-02	9.05E-03	1.11E-02

References

Bagarinao, T., 1994. Systematics, distribution, genetics and life history of milkfish, Chanos chanos. Environ. Biol. Fish 39, 23–41.

Bieber, N., Ker, J.H., Wang, X., Triantafyllidis, C., van Dam, K.H., Koppelaar, R.H., Shah, N., 2018. Sustainable planning of the energy-water-food nexus using decision making tools. Energy Policy 113, 584–607.

Cazzaniga, R., Cicu, M., Rosa-Clot, M., Rosa-Clot, P., Tina, G., Ventura, C., 2018. Floating photovoltaic plants: performance analysis and design solutions. Renew. Sust. Energ. Rev. 81, 1730–1741.

Chang, Y.-H., Ku, C.-R., Yeh, N., 2014. Solar powered artificial floating island for landscape ecology and water quality improvement. Ecol. Eng. 69, 8–16.

Choi, Y.-K., 2014. A study on power generation analysis of floating PV system considering environmental impact. International Journal of Software Engineering and Its Applications 8, 75–84.

Cruz, E.R., 1981. Acute toxicity of un-ionized ammonia to milkfish (Chanos chanos) fingerlings. Fisheries Research Journal of the Philippines 6, 33–38.

Da Silva, G.D.P., Branco, D.A.C., 2018. Is floating photovoltaic better than conventional photovoltaic? Assessing environmental impacts. Impact Assessment and Project Appraisal 36, 390–400.

Dobos, A.P., 2014. PVWatts Version 5 Manual. National Renewable Energy Laboratory (NREL).

Doherty, J., 2010. PEST Model-Independent Parameter Estimation. User Manual. :. 5th edition. Watermark Numerical Computing.

Doherty, J., Skahill, B.E., 2006. An advanced regularization methodology for use in watershed model calibration. J. Hydrol. 327, 564–577.

Durborow, R.M., Crosby, D.M., Brunson, M.W., 1997. Ammonia in Fish Ponds. Southern Regional Aquaculture Center.

Endo, A., Burnett, K., Orencio, P.M., Kumazawa, T., Wada, C.A., Ishii, A., Tsurita, I., Taniguchi, M., 2015. Methods of the water-energy-food nexus. Water 7, 5806–5830.

Endo, A., Tsurita, I., Burnett, K., Orencio, P.M., 2017. A review of the current state of research on the water, energy, and food nexus. Journal of Hydrology: Regional Studies 11, 20–30.

Ferrer-Gisbert, C., Ferrán-Gozálvez, J.J., Redón-Santafé, M., Ferrer-Gisbert, P., Sánchez-Romero, F.J., Torregrosa-Soler, J.B., 2013. A new photovoltaic floating cover system for water reservoirs. Renew. Energy 60, 63–70.

Giupponi, C., Gain, A.K., 2017. Integrated spatial assessment of the water, energy and food dimensions of the Sustainable Development Goals. Reg. Environ. Chang. 17, 1881–1893.

Granada, L., Lopes, S., Novais, S.C., Lemos, M.F., 2018. Modelling integrated multi-trophic aquaculture: optimizing a three trophic level system. Aquaculture 495, 90–97.

Hamiche, A.M., Stambouli, A.B., Flazi, S., 2016. A review of the water-energy nexus. Renew. Sust. Energ. Rev. 65, 319–331.

Handy, R.D., Poxton, M.G., 1993. Nitrogen pollution in mariculture: toxicity and excretion of nitrogenous compounds by marine fish. Rev. Fish Biol. Fish. 3, 205–241.

Hanes, R.J., Gopalakrishnan, V., Bakshi, B.R., 2018. Including nature in the food-energy-water nexus can improve sustainability across multiple ecosystem services. Resour. Conserv. Recycl. 137, 214–228.

Ho, C., Chou, W.-L., Lai, C.-M., 2015. Thermal and electrical performance of a water-surface floating PV integrated with a water-saturated MEPCM layer. Energy Convers. Manag. 89, 862–872.

Ip, Y.K., Chew, S.F., Randall, D.J., 2001. 4. In: Wright, P., Anderson, P. (Eds.), Ammonia Toxicity, Tolerance, and Excretion. Elsevier Science Publishing Co Inc.

Kougias, I., Bódis, K., Jäger-Waldau, A., Moner-Girona, M., Monforti-Ferrario, F., Ossenbrink, H., Szabó, S., 2016. The potential of water infrastructure to accommodate solar PV systems in Mediterranean islands. Sol. Energy 136, 174–182.

Kurian, M., 2017. The water-energy-food nexus: trade-offs, thresholds and transdisciplinary approaches to sustainable development. Environ. Sci. Pol. 68, 97–106.

Li, L., Yakupitiyage, A., 2003. A model for food nutrient dynamics of semi-intensive pond fish culture. Aquac. Eng. 27, 9–38.

Lin, L., Xu, F., Ge, X., Li, Y., 2018. Improving the sustainability of organic waste management practices in the food-energy-water nexus: a comparative review of anaerobic digestion and composting. Renew. Sust. Energ. Rev. 89, 151–167.

Liu, H., Krishna, V., Lun Leung, J., Reindl, T., Zhao, L., 2018. Field experience and performance analysis of floating PV technologies in the tropics. Prog. Photovolt. Res. Appl. 26, 957–967.

Loik, M.E., Carter, S.A., Alers, G., Wade, C.E., Shugar, D., Corrado, C., Jokerst, D., Kitayama, C., 2017. Wavelength-selective solar photovoltaic systems: powering greenhouses for plant growth at the food-energy-water nexus. Earth's Future 5, 1044–1053.

Lu, H.-L., Ku, C.-R., Chang, Y.-H., 2015. Water quality improvement with artificial floating islands. Ecol. Eng. 74, 371–375.

Piedrahita, R.H., Brune, D.E., Tchobanoglous, G., Orlob, G.T., 1984. A general model of the aquaculture pond ecosystem. Journal of the World Mariculture Society 15, 355–366.

Pringle, A.M., Handler, R., Pearce, J., 2017. Aquavoltaics: synergies for dual use of water area for solar photovoltaic electricity generation and aquaculture. Renew. Sust. Energ. Rev. 80, 572–584.

Sahu, A., Yadav, N., Sudhakar, K., 2016. Floating photovoltaic power plant: a review. Renew. Sust. Energ. Rev. 66, 815–824.

Santafé, M.R., Gisbert, P.S.F., Romero, F.J.S., Soler, J.B.T., Gózálvez, J.J.F., Gisbert, C.M.F., 2014. Implementation of a photovoltaic floating cover for irrigation reservoirs. J. Clean. Prod. 66, 568–570.

Silvério, N.M., Barros, R.M., Filho, G.L.T., Redón-Santafé, M., dos Santos, I.F.S., de Mello Valério, V.E., 2018. Use of floating PV plants for coordinated operation with hydropower plants: case study of the hydroelectric plants of the São Francisco River basin. Energy Convers. Manag. 171, 339–349.

Smith, D.W., Piedrahita, R.H., 1988. The relation between phytoplankton and dissolved oxygen in fish ponds. Aquaculture 68, 249–265.

Spencer, R.S., Macknick, J., Aznar, A., Warren, A., Reese, M.O., 2019. Floating photovoltaic systems: assessing the technical potential of photovoltaic systems on man-made water bodies in the continental United States. Environmental Science & Technology 53, 1680–1689.

Stein, J.S., Holmgren, W.F., Forbess, J., Hansen, C.W., 2016. PVLIB: Open source photovoltaic performance modeling functions for Matlab and Python, 2016 IEEE 43rd Photovoltaic Specialists Conference (PVSC).

Sumagaysay, N.S., 1998. Milkfish (Chanos chanos) production and water quality in brackishwater ponds at different feeding levels and frequencies. J. Appl. Ichthyol. 14, 81–85.

Svirezhev, Y., Krysanova, V., Voinov, A., 1984. Mathematical modelling of a fish pond ecosystem. Ecol. Model. 21, 315–337.

Taboada, M., Cáceres, L., Graber, T., Galleguillos, H., Cabeza, L., Rojas, R., 2017. Solar water heating system and photovoltaic floating cover to reduce evaporation: experimental results and modeling. Renew. Energy 105, 601–615.

Thurston, R.V., Russo, R.C., Vinogradov, G.A., 1981. Ammonia toxicity to fishes. Effect of pH on the toxicity of the unionized ammonia species. Environmental Science & Technology 15, 837–840.

Tian, H., Lu, C., Pan, S., Yang, J., Miao, R., Ren, W., Yu, Q., Fu, B., Jin, F.-F., Lu, Y., Melillo, J., Ouyang, Z., Palm, C., Reilly, J., 2018. Optimizing resource use efficiencies in the food–energy–water nexus for sustainable agriculture: from conceptual model to decision support system. Curr. Opin. Environ. Sustain. 33, 104–113.

Trapani, K., Millar, D.L., 2013. Proposing offshore photovoltaic (PV) technology to the energy mix of the Maltese islands. Energy Convers. Manag. 67, 18–26.

Trapani, K., Redón Santafé, M., 2015. A review of floating photovoltaic installations: 2007–2013. Prog. Photovolt. Res. Appl. 23, 524–532.

Uen, T.-S., Chang, F.-J., Zhou, Y., Tsai, W.-P., 2018. Exploring synergistic benefits of Water-Food-Energy Nexus through multi-objective reservoir optimization schemes. Sci. Total Environ. 633, 341–351.

Voinov, A., Akhremenkov, A., 1990. Simulation modeling system for aquatic bodies. Ecol. Model. 52, 181–205.

Voinov, A., Svirezhev, Y., 1984. A minimal model of eutrophication in freshwater ecosystems. Ecol. Model. 23, 277–292.

Wang, L.K., Vielkind, D., Wang, M.H., 1978. Mathematical models of dissolved oxygen concentration in fresh water. Ecol. Model. 5, 115–123.

Wolfe, J.R., Zweig, R.D., Engstrom, D.G., 1986. A computer simulation model of the solar-algae pond ecosystem. Ecol. Model. 34, 1–59.

Yao, Y., Martinez-Hernandez, E., Yang, A., 2018. Modelling nutrient flows in a simplified local food-energy-water system. Resour. Conserv. Recycl. 133, 343–353.

Zhang, T., Ban, X., Wang, X., Cai, X., Li, E., Wang, Z., Yang, C., Zhang, Q., Lu, X., 2017. Analysis of nutrient transport and ecological response in Honghu Lake, China by using a mathematical model. Sci. Total Environ. 575, 418–428.

Zhou, Y., Chang, L.-C., Uen, T.-S., Guo, S., Xu, C.-Y., Chang, F.-J., 2019. Prospect for small-hydropower installation settled upon optimal water allocation: an action to stimulate synergies of water-food-energy nexus. Appl. Energy 238, 668–682.

Zisopoulou, K., Karalis, S., Koulouri, M.-E., Pouliasis, G., Korres, E., Karousis, A., Triantafilopoulou, E., Panagoulia, D., 2018. Recasting of the WEF Nexus as an actor with a new economic platform and management model. Energy Policy 119, 123–139.